Bioactive glass scaffolds for bone regeneration and their hierarchical characterisation

J R Jones, S Lin, S Yue, P D Lee, J V Hanna, M E Smith and R J Newport

Proceedings of the Institution of Mechanical Engineers, Part H: Journal of Engineering in Medicine 2010 224: 1373
DOI: 10.1243/09544119JEIM836

Bioactive glass scaffolds for bone regeneration and their hierarchical characterisation

J R Jones[1]*, S Lin[1], S Yue[1], P D Lee[1], J V Hanna[2], M E Smith[2], and **R J Newport[3]**
[1]Department of Materials, Imperial College London, South Kensington Campus, London, UK
[2]Department of Physics, University of Warwick, Coventry, UK
[3]School of Physical Sciences, Ingram Building, University of Kent, Canterbury, UK

The manuscript was received on 9 November 2009 and was accepted after revision for publication on 10 August 2010.

DOI: 10.1243/09544119JEIM836

Abstract: Scaffolds are needed that can act as temporary templates for bone regeneration and actively stimulate vascularized bone growth so that bone grafting is no longer necessary. To achieve this, the scaffold must have a suitable interconnected pore network and be made of an osteogenic material. Bioactive glass is an ideal material because it rapidly bonds to bone and degrades over time, releasing soluble silica and calcium ions that are thought to stimulate osteoprogenitor cells. Melt-derived bioactive glasses, such as the original Bioglass® composition, are available commercially, but porous scaffolds have been difficult to produce because Bioglass and similar compositions crystallize on sintering. Sol-gel foam scaffolds have been developed that avoid this problem. They have a hierarchical pore structure comprising interconnected macropores, with interconnect diameters in excess of the 100 μm that is thought to be needed for vascularized bone ingrowth, and an inherent nanoporosity of interconnected mesopores (2–50 nm) which is beneficial for the attachment of osteoprogenitor cells. They also have a compressive strength in the range of cancellous bone. This paper describes the optimized sol-gel foaming process and illustrates the importance of optimizing the hierarchical structure from the atomic through nano, to the macro scale with respect to biological response.

Keywords: bioactive glass, scaffolds, tissue engineering, bone regeneration, NMR, XRD, nanostructure, image analysis, X-ray microtomography

1 INTRODUCTION

With 2.2 million bone graft operations carried out annually worldwide, at an approximate cost of $2.5 billion, bone is one of the most common body parts that needs repairing [**1**]. Bone defects are common due to tumour removal, trauma, or birth defects such as cleft palates. The majority of bone graft operations use autograft, harvesting the patient's own bone, usually from their pelvis. However, the amount of bone is limited and the healing of the donor site tends to take longer and be more painful than healing of the treatment site. Allogenic grafts are alternatives, e.g. irradiated bone from cadavers (bone mineral from bone banks) and demineralized bone matrix (bone mineral dissolved away using acids), but their mechanical properties are poor and there is still risk of disease transmission and rejection.

Therefore, artificial bone grafts and bone graft extension materials are needed, and there are many available on the market. The most successful are macroporous bioactive ceramic granules that the surgeon can mix with the blood of the patient and apply to the defect as a putty. The most common bioceramics used by surgeons are calcium sulphate, tricalcium phosphate (β-TCP), synthetic hydroxyapatite (HA), and biphasic calcium phosphate (a mixture of TCP and HA). Although calcium sulphate is widely used, it dissolves very rapidly *in vivo*, which can leave a new defect. TCP also dissolves rapidly, whereas HA degrades very slowly. A shift is needed

*Corresponding author: Department of Materials, Imperial College London, Prince Consort Road, South Kensington Campus, London SWT 2AZ, UK.
email: julian.r.jones@imperial.ac.uk

away from these materials to artificial grafts that can stimulate the body's natural regenerative mechanisms so that the damaged bone can be restored to its original state and function.

There are two strategies to achieve bone regeneration; *in situ* regeneration and tissue engineering. Both use scaffolds to guide and stimulate cells to produce new tissue [**2–4**]. For *in situ* bone regeneration, a scaffold must recruit the cells needed for vascularized bone regeneration, and stimulate them to produce an extracellular matrix. This means not only that the material must stimulate osteoprogenitor cells, such as mesenchymal stem cells (MSCs) to form bone, but also endothelial cells must form a network inside the scaffold to form blood vessels. Blood vessels will only grow into porous materials if the pore network is sufficiently open, and if there is cellular activity inside the pore network. A strategy for overcoming the lack of metabolic activity inside the scaffold is tissue engineering, in which cells can be seeded on a scaffold prior to implantation. MSCs can be harvested from a patient and seeded on a scaffold that acts as an active guide for three-dimensional (3D) tissue growth [**5**, **6**]. The tissue-engineered construct can then be implanted into the patient. Over time, the synthetic scaffold should resorb into the body as non-toxic degradation products, allowing the bone to remodel itself into mature bone structure. This paper concentrates on bioactive glass scaffolds designed to fulfil the role as temporary templates for both of these two strategies.

2 AN IDEAL SCAFFOLD FOR BONE REGENERATION

The general criteria for an ideal scaffold for bone regeneration are that it [**2**, **7**, **8**]:

(a) is biocompatible;
(b) forms a chemical bond to host bone;
(c) has an interconnected pore structure to allow 3D bone ingrowth;
(d) degrades at the same rate as the bone is repaired;
(e) has a surface suitable for osteogenic cell attachment;
(f) stimulates osteoprogenitor cells to produce bone matrix;
(g) exhibits mechanical properties similar to that of the host bone;
(h) can be shaped by the surgeon prior to implantation to fit the defect;
(i) has the potential to be commercially producible and sterilizable for clinical use.

Many materials are biocompatible (criterion 1), but bio-inert materials, such as titanium alloys and polymethyl methacrylate, are encapsulated by fibrous tissue after implantation, which can block bone ingrowth and cause bone loss due to micromotion of the implant. Ideally scaffolds should be made of bioactive materials (criterion 2) that encourage osteoprogenitor cell attachment (criterion 5).

There has been considerable debate regarding the minimum interconnected pore diameter required (criterion 3), and 100 μm is recognized to be the minimum interconnect diameter for a scaffold that will allow vascularized bone ingrowth. The evidence for this is that interconnects of greater than 100 μm have been found to encourage vascularization [**9**] and the minimum pore diameter for vascular bone growth into porous ceramic surfaces has been shown to be 100 μm [**10**]. The criteria for an optimized pore network for *in vitro* bone growth are less clear, especially if the scaffold undergoes degradation before implantation. Bioactive degradable materials have the potential to fulfil all criteria if they can be made into a suitable structure. Some bioactive materials can stimulate osteoprogenitor cells to produce bone matrix (criterion 6).

3 BIOACTIVE GLASS SCAFFOLDS

Bioactive glasses have been shown to bond with bone more rapidly than other bioactive ceramics [**11**, **12**] and to stimulate human osteoblast cells at the genetic level, which has been attributed to soluble silica and calcium ions being released from the glasses after implantation [**13–16**]. The bioactivity of synthetic HA has also been improved by chemical substitution of silicon (or silicate groups) for phosphorous (or phosphate groups) [**17**], which led to the development of the successful clinical product, Actifuse (Apatech Ltd, UK). This article concentrates on bioactive glasses.

Bioactive glasses are based on a covalent random network of corner-sharing silica tetrahedra containing Si-O-Si bonds. The network can be modified by the addition of network modifiers such as sodium and calcium which are ionically bonded to the network via non-bridging oxygen bonds, e.g. $Si\text{-}O^{-}\ ^{+}Na$. Phosphate is also often incorporated into the glass, although it does not form part of the silica network, it forms orthophosphate, which is charge balanced by calcium ions. The mechanism of bone

bonding to bioactive glasses is thought to be due to the formation of a carbonate-substituted hydroxycarbonate apatite (HCA) layer on the surface of the glasses following the glass corrosion processes. The HCA layer is similar to the apatite in bone and a strong bond is formed, which is thought to be due to interaction of collagen fibrils from the host bone and HCA nodules forming on the glass [**18**]. However, it could also be due to osteoprogenitor cells attaching to the surface and producing bone matrix which interacts with existing collagen fibrils.

Bioactive glasses can either be synthesized by the melt or sol-gel processes. The original bioactive glass was melt-derived (46.1 mol%, SiO_2, 24.4 mol%, Na_2O, 26.9 mol% CaO, and 2.6 mol% P_2O_5) and was named Bioglass®. It is now a commercial product in a particle form as bone filling material (Novabone®, Novabone Products LLC, Alachua, Florida) [**19**, **20**]. The clinician usually mixes the patient's blood with the particles and then pushes the putty-like mixture into the bone defect. Most recently, fine Bioglass powder ($< 5\,\mu m$) has been incorporated into many premium toothpastes under the name NovaMin® (NovaMin Technology Inc., Alachua, Florida). The aim of using NovaMin in toothpaste is to reduce tooth sensitivity by releasing the active ions to assist remineralization of microcavities in enamel, which is a biological apatite. Melt-derived glasses are made by melting oxide components in a crucible at temperatures above 1100 °C (exact temperature depends on the glass composition) and pouring into a mould (casting a shape) or quenching into water (making a frit, or powder).

The majority of methods for producing porous ceramics involve sintering and cannot be used to create porous amorphous Bioglass because of its composition. The usual method of making ceramics porous is to sinter particles into a porous block, using a template material. Often, space holders or polymer foams are used as templates [**21**]. To sinter a glass efficiently, the temperature must be above the glass transition temperature (T_g), allowing viscous flow of the glass. The problem with Bioglass is that the crystallization temperature (T_c) is very close to the T_g of the glass. Therefore, a glass-ceramic is formed, containing the canasite phase [**21**]. New compositions are being developed that can be sintered [**22**], and an alternative method for making porous scaffolds with a hierarchical pore structure similar to trabecular bone has been developed by foaming sol-gel-derived bioactive glasses [**23**].

Sol-gel-derived bioactive glasses are synthesized by the hydrolysis of alkoxide precursors to form a sol, which is a colloidal silica solution [**24**]. Figure 1 shows a flow chart of the sol-gel foaming process. A commonly used silica precursor is tetraethylorthosilicate (TEOS). Triethylphosphate (TEP) is used to add phosphate and the salt calcium nitrate is usually used to introduce calcium. The silica species in the sol then undergo polycondensation to form a network of silica (Si-O-Si bridging bonds) and is termed a gel. The gel is then heat treated to drive off the condensation by-products of water and ethanol and to remove the nitrates. The high temperature also promotes further condensation of the silica network [**25**]. Bioactive sol-gel compositions tend to be based on 58S (60 mol% SiO_2, 36 mol% CaO, and 4 mol% P_2O_5) [**26**] and 70S30C (70 mol% SiO_2 and 30 mol% CaO), but are not limited to these compositions [**27**]. Silver has also been introduced into the glasses to act as an antibacterial agent [**28**].

Sol-gel-derived bioactive glasses tend to be more bioactive and degrade more rapidly than melt-derived glasses of similar compositions. This is because sol-gel glasses have a nanometre-scale textural porosity that

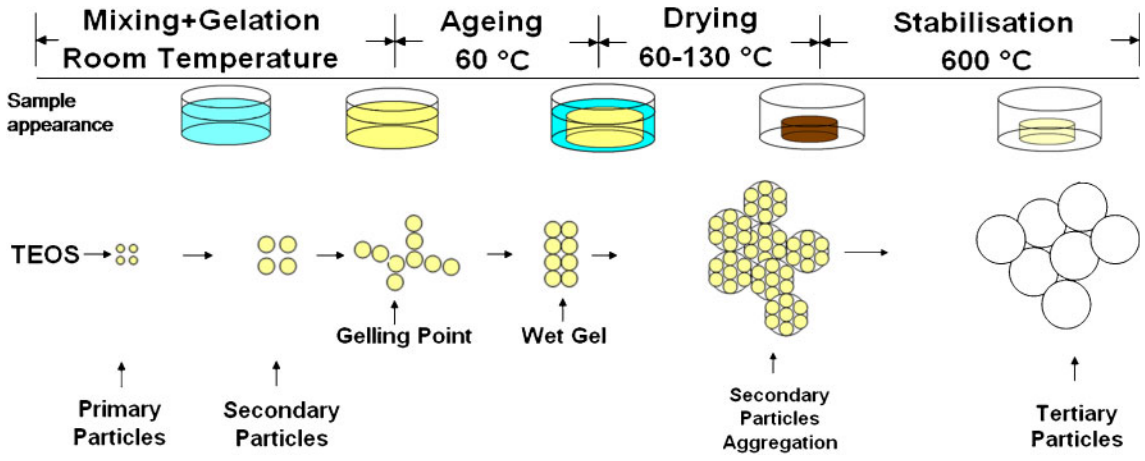

Fig. 1 Schematic of nanostructure evolution during the sol-gel process [**30**]

is inherent to the sol-gel process, which increases the specific surface area by two orders of magnitude compared to a melt-derived glass [**29**]. The textural porosity not only increases the surface area for glass corrosion by two orders of magnitude, but it also exposes many silanol groups to the solution, which act as nucleation sites for HCA layer formation. The nanopores are created due to the gelation mechanism. As condensation begins, nanoparticles of silica are formed in the sol.

These particles then agglomerate, covalently bonding as condensation continues. However, there are interstitial pores between the particles, which are filled with the condensation by-products (water and alcohol). During drying, the liquid is driven off, and during thermal processing the particles coalesce further, but some interstitial nanopores remain [**30**]. The nanopores, often termed mesopores as they are between 2 and 50 nm in diameter, are interconnected and can be tailored in size by the final sintering temperature [**8**]. The 58S composition is used in combination with Bioglass particles in NovaBone C/M, with the aim that the 58S particles will degrade rapidly, leaving spaces between the Bioglass particles to encourage bone ingrowth into the bone defect.

A foaming step can be added to the sol-gel process to produce a porous scaffold (Fig. 2). The hydrolysed sol can be foamed by vigorous agitation in air with the aid of a surfactant. The surfactant lowers the surface tension and temporally stabilizes the foam. However, in order for the process to be successful, the gelation process must be accelerated. Gelation in the conventional process is usually 3 days, but adding hydrofluoric acid (HF) can accelerate the process so that gelation occurs in minutes. This is because the fluoride forms a complex with the silica, catalysing the condensation reaction. The rapid viscosity increase assists the foaming process and the air bubbles are permanently stabilized on gelation.

The scanning electron microscope (SEM) and X-ray microtomography (μCT) images of the scaffolds (Fig. 3), show their interconnected macropores which are approximately spherical and isotropic in their distribution. This is because a good distribution of the right concentration and type of surfactant lowers the surface tension of the sol evenly throughout, so all bubbles are approximately the same size. A surfactant lowers the surface tension of the sol because it consists of molecules that have a polar (hydrophilic end) and a hydrophobic end (Fig. 4). The type of surfactant required is very dependent on the solution composition. In this case Teepol® (Thames Mead, UK) works well, which is a commercial mixture of non-ionic and ionic surfactants. Surfactant content is critical as too much will trigger micelle formation, where efficiency of the surfactant is reduced. For maximum surfactant efficiency, the sol must contain high molar ratios of excess water (R ratios greater than eight). On gelation, the bubbles are permanently stabilized as the condensation reactions form the silica network around them. The formation of Si-O-Si bonds causes shrinkage of the bubble walls, bringing neighbouring air bubbles into very close contact. During ageing and drying, the liquid drains from the points of contact and further shrinkage causes rupture of the liquid film at the points of contact, opening up the interconnects between the macropores. This is critical for bone scaffolds.

All variables in each stage of the foaming process (Figs 1 and 2) have an effect on the pore structure, including the sol (glass) composition and surfactant concentration [**31**], gelling agent concentration, the temperature at which the process is carried out, and amount of additional water used with the surfactant [**32**]. Changing the surfactant concentration while

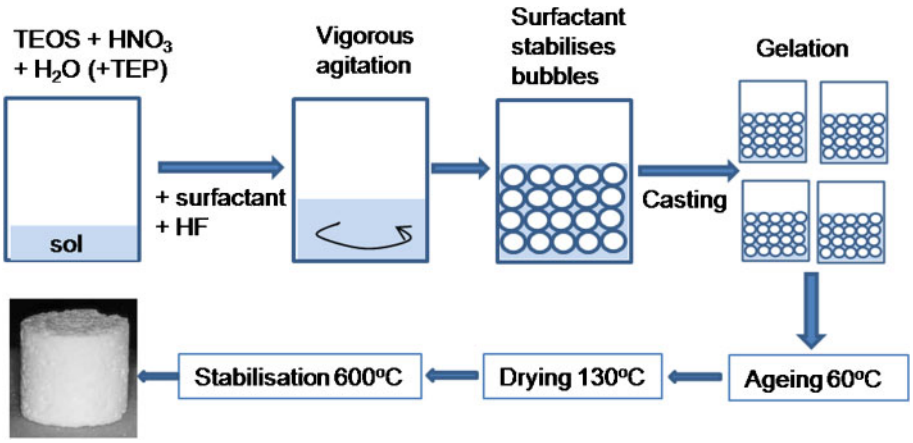

Fig. 2 A flow chart of the sol-gel foaming process

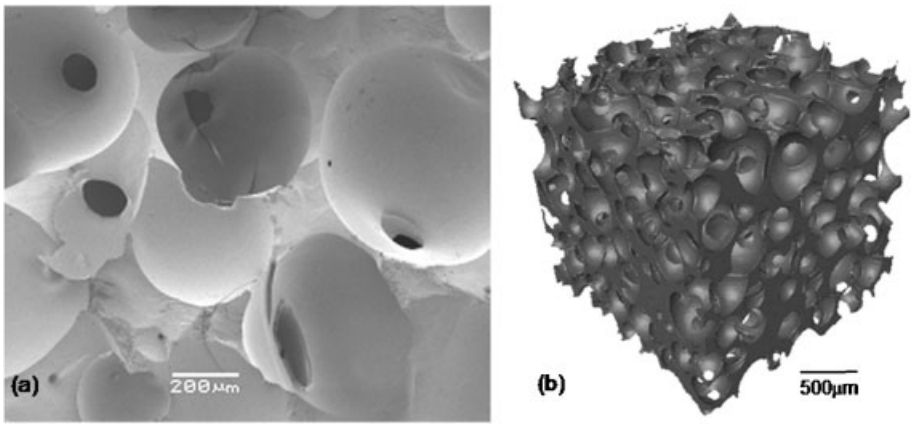

Fig. 3 Images of the macropore structure of sol-gel-derived bioactive glass foam scaffolds of the 70S30C composition (a) SEM micrograph, and (b) μCT image

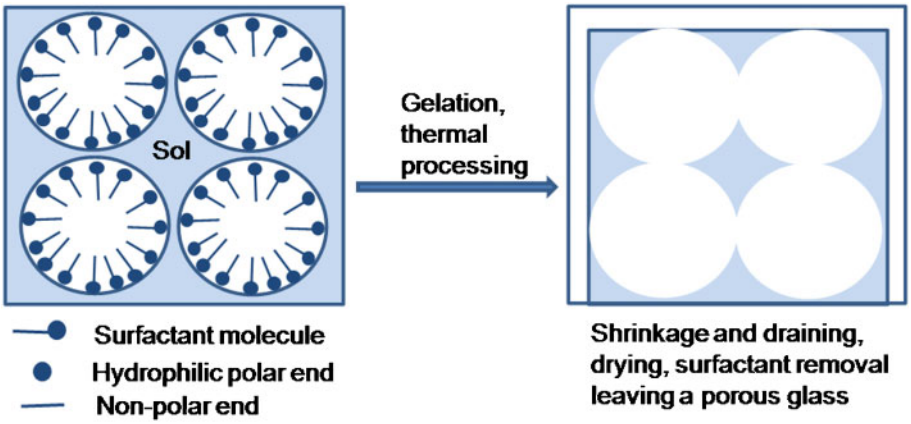

Fig. 4 Role of surfactant molecules in creating interconnected pore networks

keeping all other variables constant is the most efficient method to control the modal interconnect diameter [**31**].

4 CHARACTERIZATION OF THE MACROSTRUCTURE OF A SCAFFOLD

Whatever material is chosen as a scaffold for bone regeneration, it will need to act as a template for 3D bone and blood vessel growth. To ensure the pore structure is suitable, it is necessary to be able to quantify the pore network: imaging alone is not enough. The SEM image in Fig 3(a) shows that the foam is comprised of large macropores that are highly interconnected (dark areas). However, unless complex stereology over many images is employed, it is difficult to quantify the pore sizes from SEM images. The reasons for this are that SEM images are two-dimensional (2D) images of a fracture surface. This means that it depends where each pore was fractured as to whether the maximum diameter is imaged. From the SEM image, it appears that the pore sizes are heterogeneous. It also appears that not all the pores are interconnected, as many of interconnects are above the plane of the image. Images from μCT (Fig. 3(b)) have provided 3D images of porous materials, which give qualitative information on pore shape and heterogeneity. μCT collects a series of 2D transmission X-ray images that are reconstructed to form a 3D image. A great benefit is that the user can view through the 3D images and manually measure pores and interconnects using image analysis software. However, image analysis methods are needed that can be applied to an entire scaffold to obtain meaningful pore size distributions.

The traditional method for obtaining pore size distributions has been mercury intrusion porosimetry (MIP), which forces mercury into an evacuated sample and applies the Washburn equation [**33**] to derive a pore size distribution. The pore diameter given is the equivalent diameter of constrictions to the flow of mercury as a function of pressure applied. Disadvantages of the MIP technique are that it is

destructive (mercury contamination) and it is not possible to determine what pore size the technique is measuring, i.e. whether it is the true interconnect diameter.

μCT has the advantage of being non-destructive to most materials. However, obtaining pore size distributions of open pore structures is not trivial. Many authors rely on percentage porosity data, but it is not a useful parameter for tissue scaffolds as it does not tell the user whether the pores are large enough for tissue ingrowth. Using μCT, it has recently been shown that two bioactive glass foam scaffolds made in the same way (with the same composition), only poured into moulds at different times, can have the same percentage porosities, but one can have a heterogeneous pore structure of one large pore and smaller small pores, which is potentially unsuitable for bone regeneration, while the other can have a homogeneous structure [**34**]. The non-destructive nature of μCT makes it a useful quality assurance tool.

Complex operations are required to obtain pore size distributions from 3D images. The current authors have achieved this by applying three image processing algorithms in sequence to μCT images [**34–36**]. Figure 5 shows the procedure step by step. Figure 5(a) shows a smoothed ('thresholded') reconstructed version of the raw data. Thresholding is an important step that divides the image into its air and solid components. Initially, the macropores must be identified. This is simple for closed pores, but for this open pore structure a new dilation algorithm had to be developed [**35**]. The dilation algorithm is applied to grow from the scaffold walls into the centre of the pores, noting the number of steps it has taken to grow to each voxel (a volume pixel). The process is illustrated schematically in the pores in Fig. 5(b). When the steps converge in the centre of the pore the centroids are identified. When the dilation is carried out across the entire sample, a distance map across the sample is created as the size of each step is known. Using the centroids as starting points, a 3D watershed algorithm is applied to the distance map to divide the image into individual pores. Watershed algorithms find the set of points, considered as a

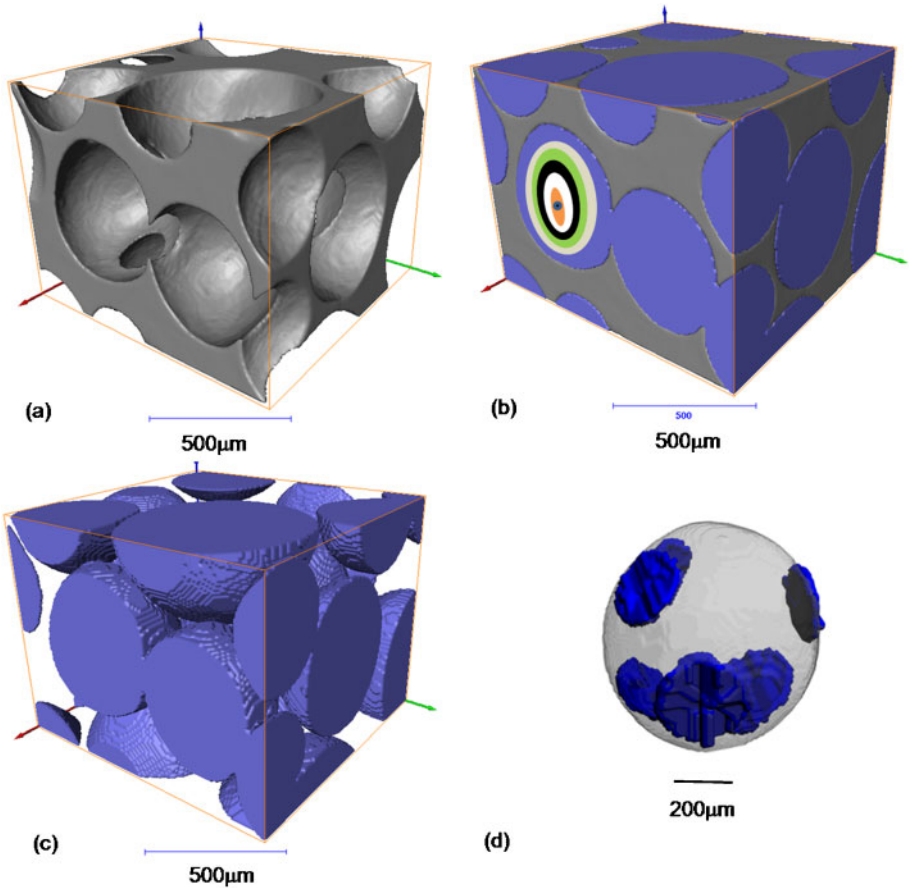

Fig. 5 Step by step process of 3D pore network quantification from μCT data (a) thresholded 3D image, (b) identification of the macropores using the dilation algorithm, (c) 3D image of identified pores without the material, and (d) an individual pore with its interconnects

height map, analogous to the watersheds of a river basin, where regions are divided regions by where water would flow to the same final point. Figure 5(c) shows the identified macropores with the scaffold image removed. Voxels with neighbours in the same two adjoining pores are then grouped and defined as interconnects. Figure 5(d) shows an individual pore and the interconnects that connect this pore to the neighbouring pores. The pores and interconnects are then quantified to determine their volume (for pores) or area (interconnects) and maximum diameter. Yue *et al.* [**34**] also added the step of using principal component analysis to improve accuracy of interconnect size.

Figure 6 compares interconnect size distributions of a 70S30C bioactive glass scaffold obtained by mercury intrusion porosimetry and μCT image analysis. The distributions show that image analysis of the μCT data determines a higher interconnect size than that measured by mercury porosimetry. This could be due to resolution limitations of the μCT (5 μm in this case), but more likely it is due to the mercury porosimetry model applied.

Another application of μCT imaging is the use of the data in macroscale models to predict properties non-destructively, based on their geometry. Permeability can be predicted in a microscale flow simulation. The predicted flow path throughout a typical scaffold can be obtained together with the applied pressure required for a scaffold to become populated by solution [**36**]. Virtual compressive testing can also be carried out by compressing a meshed 3D image (finite element model) by displacing the nodes along the top face downwards while fixing the nodes on the bottom face. The simulated load versus displacement curve can be obtained, and if the Young's modulus of the dense material is known, this value can be input into the finite element model and an effective stiffness for the porous structure can be found [**37**]. Whenever models are used, they must be validated; another advantage of μCT is that, if the chamber in the machine is large enough, *in situ* rigs for mechanical testing can be designed so that scans can be taken of materials as they are placed under compression. Transmission (2D) images can be taken continually while a material is under a constant strain rate, or 3D images can be obtained if the load is stopped for scanning [**34**, **38**]. This technique enables 3D crack paths to be imaged in and allows 2D imaging of crack initiation points.

There are some disadvantages of the μCT technique at present. First, it takes time to obtain the images and skilled users are currently needed to apply the quantification tools, which are still under development (including by the current authors). More problematic is that resolution is limited to the micron scale, especially for samples larger than 1 mm. Resolution of a high-end laboratory μCT is likely to be ~5 μm (the dimensions of a voxel) for a 5 mm cube sample. A tomography unit on a beam line of a

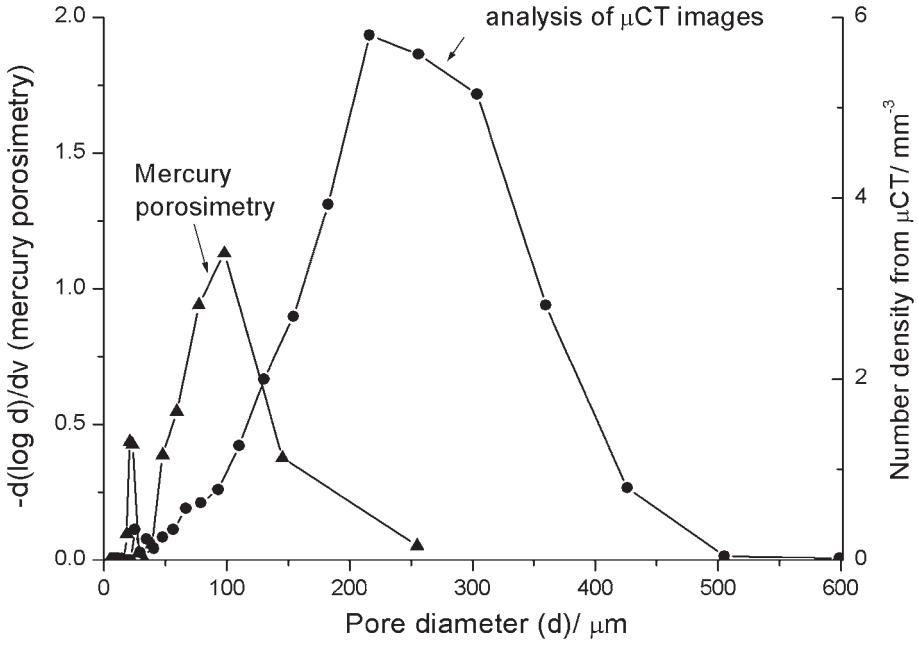

Fig. 6 Pore interconnect size distributions of a 70S30C foam scaffold obtained by mercury porosimetry (left *y*-axis) and image analysis of μCT images (number density, right *y*-axis) [**8**, **36**]

synchrotron X-ray source can give sub-micron resolution. However, despite the promise of very high resolutions, tomography is limited by the need to have the entire sample in the field of view. Therefore, the resolution is not only determined by the magnification method, but also by sample size. For example, to achieve 0.7 μm resolution on a synchrotron beam line, a cubic sample with dimensions of 1 mm was needed [**34**]. Other issues are that it is difficult to resolve two different materials if either they have very similar X-ray attenuations, or very different ones. This is of particular consequence in composite materials or scaffolds containing tissue. An example of materials with very similar attenuation is HA and bone; while an example of very different attenuations is a composite scaffold of polymer and bioactive ceramic. In the latter the ceramic phase has high X-ray attenuation and therefore shows up on an image, whereas the polymer attenuation is so low relative to the ceramic that it is difficult to distinguish it from the air in the pores. It is possible to obtain images, but resolution may be affected. In terms of quantification, the method described here is most suitable for regular pore structures with pores that can be approximated by spheres or ellipsoids. At present many highly irregular structures cannot be fully quantified so that new procedures are needed.

5 THE NANOSTRUCTURE OF A BIOACTIVE GLASS SCAFFOLD AND ITS CHARACTERIZATION

Nanoscale porosity is inherent to sol-gel-derived bioactive glasses made under acidic catalysis. Therefore, the struts of foam have a nanoporosity with diameters in the range 2–20 nm, termed mesoporosity. The mesoporosity is not ordered, but is highly interconnected. Because of the small size of the pores and the insulating nature of the material, it is difficult to image the nanopores [**30**]. A transmission electron microscope (TEM) is the only way to achieve the required resolution, but the images are effectively 2D, so it is difficult to identify the pores. The current method for measuring nanopore size in sol-gel glasses is nitrogen sorption, which obtains an isotherm of nitrogen adsorbed (and then desorbed) on a material in a vacuum at 77 K as a function of relative pressure. An example is shown in Fig. 7(a). The initial portion of the adsorption branch is approximately linear and represents a monolayer of nitrogen droplets condensing on a material. As relative pressure increases, the gradient of the curve increases as multi-layers form and a steep increase occurs when pores begin to fill. All pores are full as relative pressure reaches one [**39**]. When the isotherm is not reversible, i.e. the desorption branch does not overlay the adsorption branch, a hysteresis loop is formed, which is due to nitrogen being trapped in pores. Isotherms have been used to attribute shapes to nanopores by first assigning a type to the isotherm obtained from a test. The isotherm in Fig. 7(a) is a type-IV isotherm with a type-II hysteresis loop. According to Sing *et al.* [**39**] the isotherm would imply the material is mesoporous and the pores are approximately cylindrical (from the isotherm type), and that the pores were narrower at the ends of the cylinder than at the centre [**40**]. The inset in Fig. 7(a) illustrates the pore shape allocated to this type of isotherm. If the pores are indeed cylindrical in nature, the Barrett–Joyney–Halenda (BJH) method can be applied to the desorption branch of the isotherm to obtain a pore size distribution [**41**]. The BJH method assumes a meniscus evaporates from a cylindrical pore during desorption. An example of the distribution is shown in Fig. 7(b). The vertical axis is a derivative of the volume of nitrogen desorbed from the foam relative to the pore diameter. A field emission gun (FEG) SEM can provide nanoscale images, but only shows the highest scale structural units (condensed nanoparticles) that make up the glass. However, recent TEM and FEG-SEM (see inset in Fig. 7(b)) studies of the sol-gel process indicate that the nanopores are interstitial spaces between agglomerated and condensed (and therefore covalently bonded) nanoparticles [**30**]. Therefore, the BJH method may not be accurate, but it is the best model available. It is likely that the pores are indeed interconnected, which yields the type-IV isotherm, and that their size is $\sim$ 10–20 nm, but their shape is likely to be the irregular shapes formed between randomly packed spheres (Fig. 1).

The processing variables that affected macroporosity have little effect on the nanoporosity. One method of tailoring nanoporosity is to change the alkoxide precursors. Adding trimethylethoxysilane (TMES) to the sol has been shown to hinder some of the condensation reaction. This occurs because the hydrolysed TMES has one less reaction site than hydrolysed TEOS, so it condenses into the silica network, but then reduces the number of points that more Si-O-Si bonds can form, leading to larger pore sizes (modal pore sizes in excess of 30 nm compared to the 12 nm of conventional sol-gel glasses, Fig. 8).

Nanopore size can also be controlled by changing the final sintering temperature of the scaffolds [**8**]. Initially, the sintering temperature was chosen to be

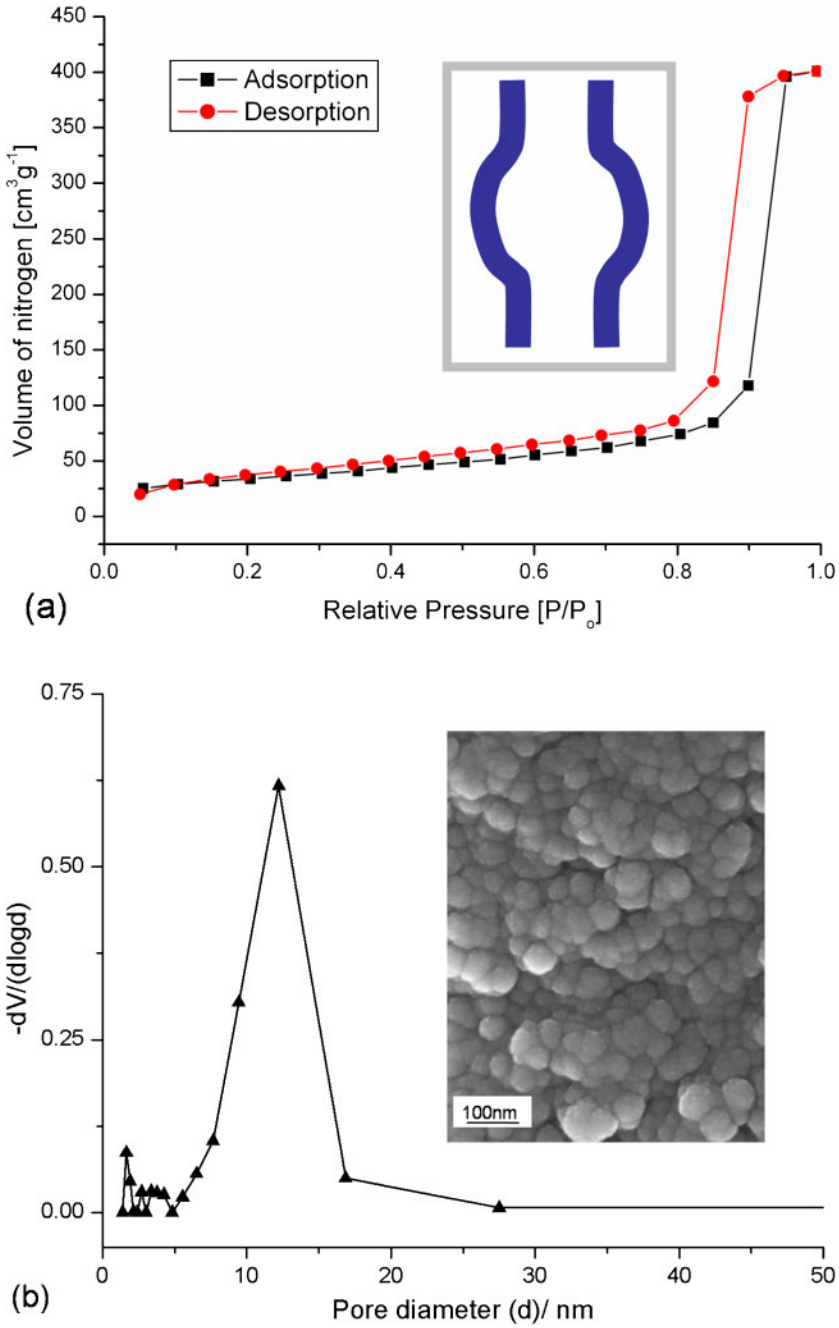

Fig. 7 Nitrogen sorption characterisation of a sol-gel derived bioactive glass scaffold (a) an isotherm with an illustration of predicted pore shape (inset), and (b) a BJH pore size distribution with a FEG-SEM image of the nanoporosity (the vertical axis is a derivative of the volume of nitrogen desorbed from the foam relative to the pore diameter)

600 °C [**23**]. This is because it was thought that the minimum temperature possible should be used to achieve the highest bioactivity. A temperature of 600 °C was chosen as the minimum because when calcium nitrate is used in the sol-gel process to introduce calcium into the glass composition, the residual nitrates must be removed to chemically stabilize the glass and make it biocompatible (non-toxic to cells). Nitrates are burnt off at approximately 550 °C. Also important is that calcium is not introduced into the network until the temperature reaches 400 °C [**30**]. As the sintering temperature increases from 700 to 800 °C, the modal pore diameter reduces from 17 nm to approximately 12 nm [**8**]. The decrease in textural porosity also results in an increase in compressive strength. Foams sintered at 600 °C have a compressive

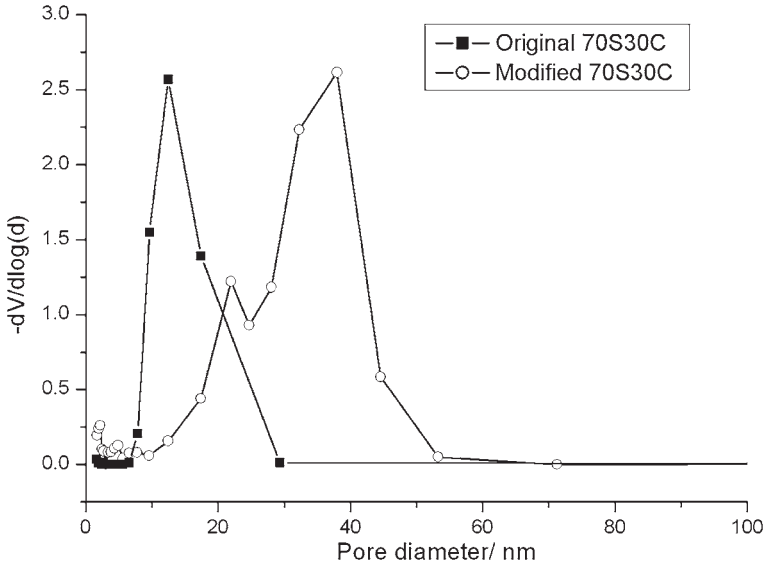

Fig. 8 BJH pore size distributions from nitrogen sorption of conventional 70S30C and 70S30C with increased nanopore sizes due to modification with TMES

strength of approximately 0.25 MPa while similar foams sintered at 800 °C have a compressive strength of approximately 2.4 MPa, similar to that of trabecular bone (2–12 MPa). Therefore, after sintering at 800 °C for 2 h, the scaffold has a modal interconnected pore diameter in excess of 100 μm and a maximum compressive strength of 2.4 MPa. However, this reduces the bioactivity and degradation rate of the scaffold. A method commonly used for the initial screening of a bioactive material is the immersion of the material in simulated body fluid (SBF). If a HA layer forms on the surface within a few days it is likely that bone will bond to the material if it is implanted. In the case of the glass foam scaffolds, the HCA layer formed in 3 days in SBF when the scaffold was sintered at 800 °C, rather than after 8 h when sintered at 600 °C. This is not necessarily due to a reduction in pore size, but rather by further condensation of the silica network. Nuclear magnetic resonance (NMR) results show that the glasses sintered at 800 °C have more bridging oxygen bonds and fewer Si-OH groups than those sintered at lower temperatures [**30**]. This illustrates the importance of atomic level characterization in addition to characterization at the nano and macro scales.

6 ATOMIC STRUCTURE OF A BIOACTIVE GLASS SCAFFOLD

The osteogenic properties of bioactive glasses are a direct result of their atomic structure. They stimulate cells by release of ions and they bond to bone via the formation of an HCA layer. The exact mechanism of formation of that layer has been the subject of much discussion. Hench and Polak [**16**] and Hench *et al.* [**18**] proposed that the layer formed by glass corrosion mechanisms: cations (Na^+, Ca^{2+}) are released from the glass as H^+ ions arrive from aqueous media; a silica-rich layer is thus formed at the glass surface; if pH rises locally above nine then Si-O-Si bonds are broken; repolymerization of Si-O-Si bonds can occur; a high concentration of Si-OH groups can trigger deposition of amorphous calcium phosphate; incorporation of OH and carbonate from the solution as the calcium phosphate crystallizes to form HCA. Hill [**42**] proposed that melt-derived glasses must have a network connectivity (average number of bridging oxygen bonds per silicon atom in the glass) of approximately two if they are to be bioactive. This is to allow silica species to be released from the glass without the breaking of Si-O-Si bonds. To have a network connectivity of two, the silica content of the glass must be approximately 50 mol%. In fact 60 mol% SiO_2 is thought to be the maximum silica content for a melt glass to be bioactive. However, sol-gel-derived glasses have been found to be bioactive with up to 80 mol% SiO_2 in their nominal composition. This is because sol-gel glasses have a high OH content. Nanoscale porosity is inherent to the sol-gel process and due to the aqueous nature of the sol the glasses have a high OH content, which changes their actual composition. Solid state magic angle spinning nuclear magnetic resonance (MAS-NMR) can be used to identify the atomic structure of glasses. One im-

portant discovery is the role of the calcium precursor and how calcium affects the evolution of the glass network and nanostructure. Calcium is a network modifier in a silica network and calcium nitrate is commonly used as a calcium precursor for sol-gel-derived bioactive glasses [**26**]. The reasoning behind its use is that it is soluble in aqueous solutions and therefore will donate calcium to the sol at low temperature as it dissociates. However, it is not that simple. Calcium nitrate does donate calcium to the silica network, but only once the material is heated to 400 °C. This has a great influence on what types of bioactive materials can be made using this process and also on the homogeneity of sol-gel glasses. Fourier transform Raman spectroscopy and isotopically enriched ^{17}O solid state NMR studies showed that calcium did not enter the silica network until the thermal processing temperature reached 350 °C [**43**], but thermal real-time X-ray diffraction (XRD), where a gel was heated from room temperature to 800°C and XRD spectra collected in real time, and MAS-NMR data revealed that calcium did not enter the silica network until the material was heated to 400 °C [**30**]. ^{29}Si NMR showed that the network connectivity of the dried gel was higher (high Q^4 content) for temperatures below 400 °C than it was above 400 °C when the calcium was incorporated as a network modifier, disrupting the silica network and increasing the Q^3 and Q^2 content [**30**]. Furthermore, the role of calcium nitrate was followed during the sol-gel process. During the mixing stage, the calcium nitrate is soluble in the sol and during condensation and gelation it remains in solution as the silica nanoparticles form and coalesce (Fig. 1). During drying, the condensation by-products (water and alcohol) are driven off and the calcium nitrate coats the silica nanoparticles. As the temperature increases above 400 °C, the calcium enters the network by diffusion and the nitrate by-products are driven off above 550 °C. Sol-gel glasses were often thought to be more homogeneous than their melt-derived equivalents, but at the atomic level they may not be, depending on the process conditions. Figure 9 shows a photograph of a cross-section of a large sol-gel monolith of the 70S30C composition, made by the conventional sol-gel method and stabilized at 600 °C. It is clear that the glass is not homogeneous. The outer region had an eight-times-higher calcium content than the central region (from secondary ion mass spectrometry) due to the calcium diffusion during thermal processing. ^{29}Si MAS-NMR showed that the region near the edge of the monolith had a ~4 per cent higher Q^2 content and ~4 per cent lower Q^4 content than the central region, due to the differing calcium content, however, this was less difference than expected. ^1H NMR showed that there was a greater difference in the -OH content [**44**]. Homogeneity can be improved by reducing monolith size and using a hydrophilic mould material. These studies show that the manufacturing method must be carefully designed to obtain homogeneous bioactive glasses and that the calcium source must be considered very carefully if lower temperature processing is employed, e.g. in the synthesis of inorganic/organic hybrids, which are a particular type of nanocomposite synthesized by introducing a polymer into the sol-gel process at the room temperature stage, prior to gelation [**45**, **46**].

Atomic structure investigations have also shed new light on the mechanism of bioactivity. Neutron diffraction with isotopic substitution (NDIS) can probe the calcium environment in great detail, obtaining information on both short and medium-range order. Conventional XRD concentrates on observed interference peaks (in *Q*-space) and is primarily of use in the context of crystalline samples, but synchrotron XRD, which uses short wavelengths and benefits from high fluxes, allows a total diffraction strategy to be adopted whereby analysis in *Q*-space and Fourier analysis of the *r*-space pair distribution provide both crystallographic (where present) and generic local order information. Combining NDIS with XRD and solid state NMR studies has given insights into the structure of sol-gel glasses and its affect on bioactivity. Neutron diffraction revealed a 70S30C sol-gel glass that the Ca–O environment comprised three distinct, but partially overlapping correlation shells centred at 2.3, 2.5, and 2.75 Å. On exposure to SBF, the glass preferentially loses the shortest length correlation [**47**]. A Ca···H

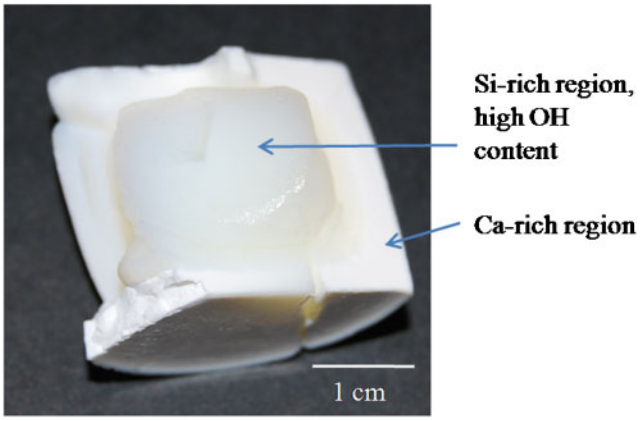

Fig. 9 Bioactive glass monolith made by the traditional sol-gel process with heterogeneity [**44**]

correlation also became evident at 2.95 Å which may be due to the lengthening of Ca–OH associated with the increased calcium coordination number, but may also be due to a Ca···H correlation in HA [**48**]. Ca X-ray absorption fine structure spectroscopy and X-ray absorption near edge structure show that the calcium oxygen environment in the sol-gel glass is six-coordinate and independent of glass composition. On reaction with SBF, the calcium coordination increases as the Ca-O bond distance increases, consistent with the formation of an HCA layer [**49**].

Synchrotron XRD experiments can be carried out on glasses previously exposed to SBF [**47**], or spectra can be collected continually with the help of a specially designed rotating sample cell [**50**]. XRD revealed that after only 30 min of exposure to SBF 75 per cent of the calcium content was lost from the bulk of the foam. Fluctuation of calcium content in the material and in the SBF was observed, showing the calcium ions continually being released from the glass and redeposited. After 1 h, whilst the underlying amorphous pattern remains, growth of calcium octacalcium phosphate (OCP) crystallites was observed, showing that OCP forms prior to HCA. By 10 h the polycrystalline calcium phosphate was replaced by a disordered phase, which continued to grow. After 25 h, poorly crystalline HA overlayed a (Ca-depleted) silicate glass [**47**]. ^{17}O NMR found rapid loss of non-bridging oxygen as calcium is leached from the glass, which supports the theory of repolymerization of Si-OH groups. Conventional XRD and Fourier transform infra red spectroscopy studies simply observe an apatite layer forming at 8 h of exposure to SBF [**8**, **51**].

These results confirmed earlier theories of an amorphous phase crystallizing to HCA, but also showed it was more complicated than originally thought. These experiments were carried out on monolithic samples. Sol-gel foam scaffolds of the same composition produced different results [**50**]. Spectra were collected continuously in SBF. After 1 h polycrystalline TCP and HA was observed and HCA after 5 h. The porosity of the material appears to have an important effect on the mechanism of formation of HCA in SBF. The nanopore size was similar (12 nm for the monoliths, 17 nm for the foams). Specific surface area and dissolution rate would have been higher for the foams.

Advanced probe techniques are therefore vital in understanding how atomic structure affects nanostructure (e.g. nanoporosity) and macroscopic properties such as degradation rate and bioactivity. It is also critical to correlate how atomic, nano and macrostructure affect cellular response.

7 CELLULAR RESPONSE TO A BIOACTIVE GLASS SCAFFOLD

Sol-gel foam bioactive glasses release soluble silica and calcium ions; hence they are expected to stimulate osteogenic cells. Primary human osteoblasts, harvested from the femoral heads removed during total hip replacements, have been cultured on bioactive glass foams of both the 58S and 70S30C compositions [**52**, **53**]. The cells attached, proliferated, and produced bone extracellular matrix (mainly collagen type I), which mineralized after 10 days of culture. This can happen on many materials in cell culture if growth factors and/or hormones (e.g. dexamethasone) are added to the culture, but no such additives were required for this to occur on the bioactive glasses, which showed their osteogenic potential. There was little difference between the two compositions, implying that phosphate in the composition had little effect on cell response. The reason for this was that characterization of the glasses at the atomic level, by MAS-NMR spectroscopy, revealed that the phosphate in 58S was not involved in the glass network. The phosphate was present as orthophosphate, which was charge balanced by calcium ions, meaning it is loosely bound into the glass and it is released into solution as soon as a glass is exposed to an aqueous solution [**31**]. When cells were cultured on 70S30C scaffolds, similar results were found to the 58S studies. Mineralized bone nodules were observed after 2 weeks of culture without supplements [**53**]. Bielby *et al.* [**54**] have also shown that the dissolution products of sol-gel-derived bioactive glasses can trigger murine embryonic stem cell differentiation into osteogenic cells. These results confirmed that it is combinations of soluble silica and calcium ions released from the scaffold that stimulate the cells.

8 SUMMARY

Bioactive sol-gel foam scaffolds have the potential to serve as scaffolds for bone regeneration and bone tissue engineering applications. The process can produce scaffolds with interconnected macropores (300–600 μm in diameter) with interconnects in excess of 100 μm. The scaffolds are degradable, bioactive, and have compressive strengths similar to porous bone. As they degrade they release soluble silica and calcium ions that can stimulate bone growth. They have a hierarchical pore structure of interconnected macropores and an inherent nanoporosity. Both scales of pores can be tailored independently. It is important to

optimize scaffolds such as these from the atomic through nano to macro scale with respect to cell response because the atomic structure affects bioactivity and degradation rate, the nanoporosity affects surface area, degradation rate, and cellular attachment and the macropore structure affects cell behaviour and tissue ingrowth. μCT can be used in conjunction with 3D image analysis to quantify the macropore network and to non-destructively predict fluid flow within the scaffold and its mechanical properties. These techniques can be applied to many scaffold materials. Nanopores have to be quantified using gas sorption techniques. Further development of tomography techniques are required to enable imaging of cells within scaffolds. The image analysis procedures also need to be improved so that they are automated and user friendly, and applicable to random pore network architectures. The fullest understanding of the behaviour of these materials was only possible through an integrated use of a large range of physical probe techniques.

ACKNOWLEDGEMENTS

The EPSRC (GR/T26344, EP/E057098/1, EP/050611/1, EP/E051669/1, GR/R57492, EP/C004671/1), Royal Academy of Engineering, and Philip Leverhulme Prize for financial support and STFC for access to neutron and X-ray facilities and their beamline scientists for help and support in collecting the data.

REFERENCES

1 **Giannoudis, P. V., Dinopoulos, H.,** and **Tsiridis, E.** Bone substitutes: an update. *Injury-Int. J. Care Inj.*, 2005, **36**(S3), 20–27.
2 **Holy, C. E., Shoichet, M. S.,** and **Davies, J. E.** Engineering three-dimensional bone tissue *in vitro* using biodegradable scaffolds: investigating initial cell-seeding density and culture period. *J. Biomed. Mater. Res.*, 2000, **51**(3), 376–382.
3 **Langer, R.** and **Vacanti, J. P.** Tissue engineering. *Science*, 1993, **260**(5110), 920–926.
4 **Lavik, E.** and **Langer, R.** Tissue engineering: current state and perspectives. *Appl. Microbiol. Biotechnol.*, 2004, **65**(1), 1–8.
5 **Ohgushi, H.** and **Caplan, A. I.** Stem cell technology and bioceramics: from cell to gene engineering. *J. Biomed. Mater. Res.*, 1999, **48**(6), 913–927.
6 **Takezawa, T.** A strategy for the development of tissue engineering scaffolds that regulate cell behavior. *Biomaterials*, 2003, **24**(13), 2267–2275.
7 **Jones, J. R.** and **Hench, L. L.** Regeneration of trabecular bone using porous ceramics. *Curr. Opin. Solid State Mater. Sci.*, 2003, **7**(4–5), 301–307.
8 **Jones, J. R., Ehrenfried, L. M.,** and **Hench, L. L.** Optimising bioactive glass scaffolds for bone tissue engineering. *Biomaterials*, 2006, **27**(7), 964–973.
9 **Okii, N., Nishimura, S., Kurisu, K., Takeshima, Y.,** and **Uozumi, T.** *In vivo* histological changes occurring in hydroxyapatite cranial reconstruction - case report. *Neurol. Med. Chir.*, 2001, **41**(2), 100–104.
10 **Hulbert, S. F., Morrison, S. J.,** and **Klawitte, J. J.** Tissue reaction to three ceramics of porous and non-porous structures. *J. Biomed. Mater. Res.*, 1972, **6**(5), 347–374.
11 **Oonishi, H., Kushitani, S., Yasukawa, E., Iwaki, H., Hench, L. L., Wilson, J., Tsuji, E. I.,** and **Sugihara, T.** Particulate bioglass compared with hydroxyapatite as a bone graft substitute. *Clin. Orthop. Relat. Res.*, 1997, **334**, 316–325.
12 **Oonishi, H., Hench, L. L., Wilson, J., Sugihara, F., Tsuji, E., Matsuura, M., Kin, S., Yamamoto, T.,** and **Mizokawa, S.** Quantitative comparison of bone growth behavior in granules of Bioglass(R), A-W glass-ceramic, and hydroxyapatite. *J. Biomed. Mater. Res.*, 2000, **51**(1), 37–46.
13 **Xynos, I. D., Edgar, A. J., Buttery, L. D. K., Hench, L. L.,** and **Polak, J. M.** Ionic products of bioactive glass dissolution increase proliferation of human osteoblasts and induce insulin-like growth factor II mRNA expression and protein synthesis. *Biochem. Biophys. Res. Commun.*, 2000, **276**(2), 461–465.
14 **Xynos, I. D., Hukkanen, M. V. J., Batten, J. J., Buttery, L. D., Hench, L. L.,** and **Polak, J. M.** Bioglass(R) 45S5 stimulates osteoblast turnover and enhances bone formation *in vitro*: implications and applications for bone tissue engineering. *Calcif. Tissue Int.*, 2000, **67**(4), 321–329.
15 **Xynos, I. D., Edgar, A. J., Buttery, L. D. K., Hench, L. L.,** and **Polak, J. M.** Gene-expression profiling of human osteoblasts following treatment with the ionic products of Bioglass(R) 45S5 dissolution. *J. Biomed. Mater. Res.*, 2001, **55**(2), 151–157.
16 **Hench, L. L.** and **Polak, J. M.** Third-generation biomedical materials. *Science*, 2002, **295**(5557), 1014–1017.
17 **Patel, N., Best, S. M., Bonfield, W., Gibson, I. R., Hing, K. A., Damien, E.,** and **Revell, P. A.** A comparative study on the in vivo behavior of hydroxyapatite and silicon substituted hydroxyapatite granules. *J. Mater. Sci., Mater. Med.*, 2002, **13**(12), 1199–1206.
18 **Hench, L. L., Splinter, R. J., Allen, W. C.,** and **Greenlee, T. K.** Bonding mechanisms at the interface of ceramic prosthetic materials. *J. Biomed. Mater. Res.*, 1971, **5**(6), 117–141.
19 **Hench, L. L.** Bioceramics - from concept to clinic. *J. Am. Ceram. Soc.*, 1991, **74**(7), 1487–1510.
20 **Bielby, R. C., Christodoulou, I. S., Pryce, R. S., Radford, W. J. P., Hench, L. L.,** and **Polak, J. M.** Time- and concentration-dependent effects of

dissolution products of 58S sol-gel bioactive glass on proliferation and differentiation of murine and human osteoblasts. *Tissue Engng*, 2004, **10**(7–8), 1018–1026.

21 **Chen, Q. Z. Z., Thompson, I. D.,** and **Boccaccini, A. R.** 45S5 Bioglass(R)-derived glass-ceramic scaffolds for bone tissue engineering. *Biomaterials*, 2006, **27**(11), 2414–2425.

22 **Elgayar, I., Aliev, A. E., Boccaccini, A. R.,** and **Hill, R. G.** Structural analysis of bioactive glasses. *J. Non-Cryst. Solids*, 2005, **351**(2), 173–183.

23 **Sepulveda, P., Jones, J. R.,** and **Hench, L. L.** Bioactive sol-gel foams for tissue repair. *J. Biomed. Mater. Res.*, 2002, **59**(2), 340–348.

24 **Hench, L. L.** and **West, J. K.** The sol-gel process. *Chem. Rev.*, 1990, **90**(1), 33–72.

25 **Brinker, J.** and **Scherer, G. W.** *Sol-gel science: the physics and chemistry of sol-gel processing*, 1990 (Academic Press, Boston, Massachusetts).

26 **Li, R., Clark, A. E.,** and **Hench, L. L.** An investigation of bioactive glass powders by sol-gel processing. *J. Appl. Biomater.*, 1991, **2**(4), 231–239.

27 **Saravanapavan, P.** and **Hench, L. L.** Mesoporous calcium silicate glasses. I. Synthesis. *J. Non-Cryst. Solids*, 2003, **318**(1–2), 1–13.

28 **Bellantone, M., Williams, H. D.,** and **Hench, L. L.** Broad-spectrum bactericidal activity of Ag_2O-doped bioactive glass. *Antimicrob. Agents Chemother.*, 2002, **46**(6), 1940–1945.

29 **Sepulveda, P., Jones, J. R.,** and **Hench, L. L.** *In vitro* dissolution of melt-derived 45S5 and sol-gel derived 58S bioactive glasses. *J. Biomed. Mater. Res.*, 2002, **61**(2), 301–311.

30 **Lin, S., Ionescu, C., Pike, K. J., Smith, M. E.,** and **Jones, J. R.** Nanostructure evolution and calcium distribution in sol-gel derived bioactive glass. *J. Mater. Chem.*, 2009, **19**(9), 1276–1282.

31 **Jones, J. R.** and **Hench, L. L.** Effect of surfactant concentration and composition on the structure and properties of sol-gel-derived bioactive glass foam scaffolds for tissue engineering. *J. Mater. Sci.*, 2003, **38**(18), 3783–3790.

32 **Jones, J. R.** and **Hench, L. L.** Factors affecting the structure and properties of bioactive foam scaffolds for tissue engineering. *J. Biomed. Mater. Res. B, Appl. Biomater.*, 2004, **68**(1), 36–44.

33 **Washburn, E. W.** The dynamics of capillary flow. *Phys. Rev.*, 1921, **17**, 273–283.

34 **Yue, S., Lee, P. D., Poologasundarampillai, G., Yao, Z., Rockett, P., Mitchell, C. A., Konerding, M. A.,** and **Jones, J. R.** Synchrotron X-ray microtomography for assessment of bone tissue scaffolds. *J. Mater. Sci., Mater. Med.*, 2010, **21**, 847–853.

35 **Atwood, R. C., Jones, J. R., Lee, P. D.,** and **Hench, L. L.** Analysis of pore interconnectivity in bioactive glass foams using X-ray microtomography. *Scripta Mater.*, 2004, **51**(11), 1029–1033.

36 **Jones, J. R., Poologasundarampillai, G., Atwood, R. C., Bernard, D.,** and **Lee, P. D.** Non-destructive quantitative 3D analysis for the optimisation of tissue scaffolds. *Biomaterials*, 2007, **28**, 1404–1413.

37 **Jones, J. R., Lee, P. D.,** and **Hench, L. L.** Hierarchical porous materials for tissue engineering. *Phil. Trans. R. Soc. A*, 2006, **364**(1838), 263–281.

38 **Singh, R., Lee, P. D., Lindley, T. C., Kohlhauser, C., Hellmich, C., Bram, M., Imwinkelried, T.,** and **Dashwood, R. J.** Characterization of the deformation behavior of intermediate porosity interconnected Ti foams using micro-computed tomography and direct finite element modeling. *Acta Biomater.*, 2010, **6**(6), 2342–2351.

39 **Sing, K. S. W., Everett, D. H., Haul, R. A. W., Moscou, L., Pierotti, R. A., Rouquerol, J.,** and **Siemieniewska, T.** Reporting physisorption data for gas solid systems with special reference to the determination of surface-area and porosity (recommendations 1984). *Pure Appl. Chem.*, 1985, **57**(4), 603–619.

40 **Saravanapavan, P.** and **Hench, L. L.** Mesoporous calcium silicate glasses. II. Textural characterisation. *J. Non-Cryst. Solids*, 2003, **318**(1–2), 14–26.

41 **Barrett, E. P., Joyney, L. G.,** and **Halenda, P. P.** The determination of pore volume and area distributions in porous substances: computations from nitrogen isotherms. *J. Am. Chem. Soc.*, 1951, **73**(5), 373–380.

42 **Hill, R.** An alternative view of the degradation of bioglass. *J. Mater. Sci. Lett.*, 1996, **15**(13), 1122–1125.

43 **Skipper, L. J., Sowrey, F. E., Rashid, R., Newport, R. J., Lin, Z.,** and **Smith, M. E.** X-ray diffraction and solid state NMR studies of the growth of hydroxyapatite on bioactive calcia : silica sol-gel glasses. *Phys. Chem. Glass.*, 2005, **46**(4), 372–376.

44 **Lin, S., Ionescu, C., Baker, S., Smith, M. E.,** and **Jones, J. R.** Characterisation of the inhomogeneity of sol-gel-derived SiO_2-CaO bioactive glass and a strategy for its improvement. *J. Sol-Gel Sci. Technol.*, 2010, **53**(2), 255–262.

45 **Mahony, O.** and **Jones, J. R.** Porous bioactive nanostructured scaffolds for bone regeneration: a sol-gel solution. *Nanomedicine*, 2008, **3**(2), 233–245.

46 **Jones, J. R.** New trends in bioactive scaffolds: the importance of nanostructure. *J. Eur. Ceram. Soc.*, 2009, **29**(7), 1275–1281.

47 **Skipper, L. J., Sowrey, F. E., Pickup, D. M., Drake, K. O., Smith, M. E., Saravanapavan, P., Hench, L. L.,** and **Newport, R. J.** The structure of a bioactive calcia-silica sol-gel glass. *J. Mater. Chem.*, 2005, **15**(24), 2369–2374.

48 **Newport, R. J., Skipper, L. J., FitzGerald, V., Pickup, D. M., Smith, M. E.,** and **Jones, J. R.** *In vitro* changes in the structure of a bioactive calcia-silica sol-gel glass explored using isotopic substitution in neutron diffraction. *J. Non-Cryst. Solids*, 2007, **353**(18–21), 1854–1859.

49 **Skipper, L. J., Sowrey, F. E., Pickup, D. M., Fitzgerald, V., Rashid, R., Drake, K. O., Lin, Z. J., Saravanapavan, P., Hench, L. L., Smith, M. E.,** and **Newport, R. J.** Structural studies of bioactivity in

sol-gel-derived glasses by X-ray spectroscopy. *J. Biomed. Mater. Res. A*, 2004, **70**(2), 354–360.

50 FitzGerald, V., Drake, K. O., Jones, J. R., Smith, M. E., Honkimaki, V., Buslaps, T., Kretzschmer, M., and **Newport, R. J.** *In situ* high-energy X-ray diffraction study of a bioactive calcium silicate foam immersed in simulated body fluid. *J. Synchrotron Radiat.*, 2007, **14**(6), 492–499.

51 Saravanapavan, P., Jones, J. R., Pryce, R. S., and **Hench, L. L.** Bioactivity of gel-glass powders in the CaO-SiO_2 system: a comparison with ternary (CaO-P_2O_5-SiO_2) and quaternary glasses (SiO_2-CaO-P_2O_5-Na_2O). *J. Biomed. Mater. Res. A*, 2003, **66**(1), 110–119.

52 Gough, J. E., Jones, J. R., and **Hench, L. L.** Nodule formation and mineralisation of human primary osteoblasts cultured on a porous bioactive glass scaffold. *Biomaterials*, 2004, **25**(11), 2039–2046.

53 Jones, J. R., Tsigkou, O., Coates, E. E., Stevens, M. M., Polak, J. M., and **Hench, L. L.** Extracellular matrix formation and mineralization of on a phosphate-free porous bioactive glass scaffold using primary human osteoblast (HOB) cells. *Biomaterials*, 2007, **28**(21), 1653–1663.

54 Bielby, R. C., Pryce, R. S., Hench, L. L., and **Polak, J. M.** Enhanced derivation of osteogenic cells from murine embryonic stem cells after treatment with ionic dissolution products of 58S bioactive sol-gel glass. *Tissue Engng*, 2005, **11**(3–4), 479–488.